# ScFv-modified graphene-coated IDE-arrays for 'label-free' screening of cardiovascular disease biomarkers in physiological saline

Peer-reviewed author version

DELLE, Lotta; Pachauri, Vivek; Sharma, Shikha; Shaforost, Olena; Ma, Hui; Adabi, Mohammad; Lilischkis, Rainer; WAGNER, Patrick; THOELEN, Ronald; Klein, Norbert; O'Kennedy, Richard & Ingebrandt, Sven (2018) ScFv-modified graphene-coated IDE-arrays for 'label-free' screening of cardiovascular disease biomarkers in physiological saline. In: BIOSENSORS & BIOELECTRONICS, 102, p. 574-581.

DOI: 10.1016/j.bios.2017.12.005
Handle: http://hdl.handle.net/1942/28635

# ScFv-modified Graphene-coated IDE-arrays for 'label-free' screening of cardiovascular disease biomarkers in physiological saline

Lotta E. Delle[1], Vivek Pachauri*[1], Shikha Sharma[2], Olena Shaforost[3], Hui Ma[2], Mohammad Adabi[3], Rainer Lilischkis[1], Patrick Wagner[4], Ronald Thoelen[5], Norbert Klein[3], Richard O'Kennedy[2], Sven Ingebrandt[1]

1. Department of Informatics and Microsystem Technology, University of Applied Sciences Kaiserslautern, Amerikastraße 10, 66482 Zweibrücken, Germany

2. School of Biotechnology Dublin City University, Glasnevin, Dublin 9, Ireland

3. Department of Materials, Imperial College London, South Kensington, London SW7 2AZ, United Kingdom

4. Soft-Matter Physics and Biophysics Section Department of Physics and Astronomy, Katholieke Universiteit Leuven, Leuven, Belgium

5. Hasselt University, Wetenschapspark 1, 3590 Diepenbeek, Belgium

*Corresponding author: pachauri.vivek@gmail.com; vivek.pachauri@hs-kl.de*

*KEYWORDS: IDE-arrays, Graphene, Biosensor, Cardiovascular, Electrical sensing, Physiological buffer*

## Abstract

Heart-type fatty-acid binding protein (h-FABP) and myeloperoxidases (MPO) are associated with many chronic conditions in humans and are already considered to be potentially important biomarkers for diagnosis of cardiac diseases. Here we describe a new electrical sensor platform for label-free and ultrafast screening of h-type FABP and MPO based on the use of graphene-coated interdigitated electrode arrays (IDE-arrays). Arrays of nanoscale (nanoIDE) and microscale (microIDE) electrodes were fabricated on wafer-scale by the combination of nanoimprint and photolithography processes. Chemical vapor deposition grown multilayer graphene was transferred onto these arrays to assemble the sensor platform. Biofunctional layers of novel anti-h-FABP and anti-MPO single-chain antibody fragments (scFv) were formed on the sensor platform for detection of h-FABP and MPO, respectively, in physiological saline. The advantage of using scFv fragments for enhanced detection is also shown by increased sensitivity in comparison to the competitive, state-of-the-art ELISA methods with limits of detection down to pg/ml concentrations for h-type FABP and MPO. The use of the highly specific scFv as receptor molecules on our graphene-coated IDE sensors enabled large dynamic ranges over clinically relevant concentrations for these two important cardiac biomarkers.

## Introduction

In recent surveys cardiovascular diseases (CVDs) remain the leading cause of mortality in human populations worldwide.[1] Over 17 million CVD-related deaths worldwide account for 30 percent of total death with coronary problems and heart strokes having equal percentages. CVD related deaths are more prevalent in populations with low and mid-level incomes across the globe being responsible for three quarters of total deaths. CVDs are also the leading cause of deaths by number in high income groups thus putting a significant burden on healthcare systems across the globe.[2] The risk stratification and diagnosis of cardiovascular conditions has significantly evolved over the years and has helped to accomplish major therapeutic developments in this field.[3] The prediction models for the CVDs and, therefore, the related medical intervention still remain dependent on demographical studies of physical symptoms such as diet, smoking, life-style, level of cholesterol and prevalence of diabetes. Interestingly, it is also reported that up to 20 percent of the patients may not identified with such prediction models.[4] To address these shortcomings, concerted efforts are invested in the discovery of novel biomarkers and establishing updated disease prediction and stratification matrices for the patients with high incidences of traditional risk symptoms in addition to patients that show little or no such symptoms before the onset of the disease. Novel molecular biomarkers related to various pathophysiological processes such as myocardial injury, inflammation, plaque formation/rupture, myocardial abnormalities, platelets and neuro-hormonal activation have been identified in recent years. Such developments may serve as building blocks of future therapeutic strategies and drug-discovery for CVDs.[5-8] Out of numerous molecular biomarkers identified with such pathophysiological processes, biomarkers such as C-reactive proteins (CRP), h-type fatty acid binding proteins (FABP), Growth-differentiation factor-15, pregnancy-associated plasma protein-A (PAPP-A), highly sensitive troponin (hTp), heart-type myeloperoxidase (MPO), B□type natriuretic peptide (BNP) and its deriative, N-terminal natriuretic peptide (NT-proBNP), are some of the leading candidates relevant for prognosis and diagnosis of cardiovascular problems.[9-12]

The successful use of such new molecular biomarkers for clinical assays and especially in high-risk patients demands the realization of high performance sensor platforms for molecular detection in

biological or physiological media. Varying clinically relevant ranges and low concentration levels of CVD biomarkers make their high-sensitivity and reliable screening a challenging task. Here, state-of-the-art optical detection techniques perform on the borderline for most common CVD biomarkers and improvements in their performances or alternative detection strategies are definitely required to develop future assays with a minimal cost burden. The use of specially engineered detector molecules such as single chain fragment variable (scFv) antibodies as bioreceptor layers for effective binding of the target biomarker analytes and cheaper production methods have provided a unique solution for the improvement of state-of-the-art optical detection techniques.[13-16] In parallel, the rise of high-performance electrical detection strategies arising due to the development of micro-/nano-electrochemical transducer platforms, in recent years, has started to deliver the promise of bringing clinical assays out of centralized labs by –generating miniaturized point-of-care sensor platforms for future medical diagnostics.[17-19]

In this work, we present a new electrochemical sensor platform based on the use of graphene as a nanomaterial transducer combined with newly designed scFv as the biofunctional layer for efficient binding of h-type FABP and MPO. A graphene transducer layer grown in a chemical vapor deposition process was transferred on to nanoscale interdigitated electrode arrays (nanoIDE-arrays) and microscale interdigitated electrode arrays (microIDE-arrays). Graphene surfaces were further modified with anti-myeloperoxidase (anti-MPO) and anti-fatty acid binding protein (anti-FABP) scFv. The sensors were integrated in a 16 channel, fluidic chip design to form the miniaturized biosensor platform. With this sensor approach we demonstrate the 'label-free' impedimetric detection of biomarker analytes (MPO and FABP) in physiological buffer at concentrations in clinically relevant ranges. Varying the analyte concentrations from 1pg.ml$^{-1}$ to 3µg.ml$^{-1}$, our scFv-modified, graphene coated IDE-arrays exhibited very reliable and wide sensor dynamic ranges spanning analyte concentrations from pg.-ml$^{-1}$ to µg.ml$^{-1}$. We achieved low limits-of-detection down to pg.ml$^{-1}$ concentrations for both biomarkers. Increased sensor performance of the newly designed anti-MPO and anti-FABP scFv was tested by inhibitory concentration (IC50) analysis using competitive enzyme-linked immunosorbent assays (ELISA) and showed improved sensor performances compared

to similar state-of-the-art assays. The use of such scFvs on electrical sensors, as presented in our work to produce high-sensitivity and reliable screening platforms are expected to ideally serve as a generic pathway for the further development of low-cost, clinical assays for CVD biomarkers. Further optimization and assembly of such miniaturized point-of-care screening tools are highly advantageous for accessing reliable information on the prognosis of CVDs to inform timely interventions and prevention of fatal conditions in high risk patients.[20]

## Results and Discussion

Single chain fragment variable antibody fragments (scFv) consist of immunoglobulin domains joined by a peptide link offer many advantages over conventional antibodies such as enhanced affinity and specificity against antigens.[21] The use of scFv-antibodies has become an established technique for synthesis of immunotoxins, anticancer intrabodies and applications such as therapeutic gene delivery and cancer-treatment thereby opening up new possibilities in diagnosis and disease control.[22] Synthesis of newly designed scFv antibody fragments such as anti-FABP and anti-MPO can provide significant advances towards accurate detection of ischemic disease biomarkers such as FABP and MPO, which together with several other biomarkers representing various ischemic conditions, can be directly screened from the blood. The assembly of the graphene- based sensor platform is illustrated in figure 1. The IDE-arrays working as *source* and *drain* electrodes were fabricated on 4-inch $Si/SiO_2$ wafers using a top-down lithography approach combining nanoimprint lithography and photolithography methods. Figures 1a and 1b show scanning electron microscopy (SEM) images of the typical nanoIDE-arrays and microIDE-arrays on the sensor chips. NanoIDE-arrays and microIDE-arrays with finger width of 600 nm and 6 μm were separated with 600 nm and 6 micron interdigital gaps, respectively. Each sensor chip contained 16 of these source-drain pairs containing well defined nanoIDE-arrays and microIDE-arrays with regular interdigital source-drain gaps working eventually as an '*electrical channel'* or *'transducers'* after graphene transfer. The source-drain pairs were surface passivated with a 450 nm thick passivation layer ($SiO_2$-$Si_3N_4$-$SiO_2$) in the contact-line regions in order to minimize interactions with the analytes as well as to define the transducer area, as can be clearly seen in the SEM scan images 1a and 1b. The solution-mediated CVD graphene transfer process is illustrated in figure 1C, which employed polystyrene as a support for graphene. In order to ascertain the detailed topographical features of the graphene-coated nanoIDE-array and microIDE-array sensor platforms, the sensor chips were characterized by atomic force microscopy (AFM) and Raman microscopy techniques. Figure 2 shows the surface characterization of typical sensor chips and, subsequently, the surface modified, graphene-coated IDE-arrays with anti-MPO and anti-FAB scFv as biofunctional layers. Figure 2a shows an AFM image of a typical nanoIDE-array coated with

graphene. The graphene layer can be clearly seen to completely cover the nanoIDE-array while extending onto the passivation layer. Graphene transfer on the passivated electrode array therefore limits the transducer area to the passivation window and consequently helps to minimize device-to-device variation in sensor characteristics. A zoomed in AFM scan image on the right side shows the transducer area and the nanoIDE-array covered with graphene. The thickness of the graphene layer was determined to be around 8 to 10 nm (SI6) corresponding to 10 to 15 layers.[23] Figure 2b shows the Raman microscopic characterization of the graphene layer directly on the sensor platform (inset image). The graph shown in the image represents a typical Raman spectrum for multilayered graphene.[24] The higher G-band intensities (1565 $cm^{-1}$), presence of a faint D peak (1132 $cm^{-1}$) and a low intensity 2D peak (2670 $cm^{-1}$) can be attributed to a disordered lattice, defects and folding of multilayers during the growth or transfer process.[24-27] G-peak intensity for the multilayer Graphene transferred onto the nanoIDE-array is shown in the optical image in figure 2b. The inhomogeneous spatial distribution of the intensity may be due to the folding of graphene multilayers. The graphene-coated IDE-arrays were then functionalized with either anti-MPO or anti-FABP scFv as receptor molecules. The schematics shown in figure 2c and 2d illustrate the realization of the biofunctional layer. The immobilization process details are given in the methods section. Figure 2e shows the AFM image of a sample device after biofunctionalization. As compared to the graphene-coated IDE-arrays in shown in figure 2a, the antibody fragment scan be clearly seen in the AFM image, distributed over the graphene layer forming granular and agglomerated structures. The assembled sensor platform was mounted on a specially designed polymer circuit board (PCB) and integrated with a fluidic reservoir on top to carry out the electrical bioassays.

It is worth mentioning that there is a significant surge in the reporting of label-free electrical biosensor concepts in recent years based on the use of one-dimensional (1D) and two-dimensional (2D) materials as transducers and the accompanying impressive sensor performances.[28-29] However, implementation of such nanoscale sensor platform for real applications requires overcoming several technological and economic thresholds such as ability to detect clinically relevant analyte concentrations in complex biological matrices and scalable production remain major concerns.[30-31]

Other than the use of highly-sensitive and versatile nanomaterial transducers and novel top-down nanofabrication approaches able to solve sensor reproducibility issues, realization of optimal biofunctional layers has often been overlooked and remains a key challenge in deploying sensor concepts for real applications.[32-33] Engineering of novel biomolecules and biomolecular interfaces has become an important aspect of developing highly efficient screening methods and biomolecular assays.[34-36] Production of scFv for realizing more efficient immunoassays has also become a wide-spread practice in clinical immunology because of their easier production methods, stability and highly specific binding to the target analytes.[22, 37] Here we synthesized scFv to use as an efficient biofunctional layer for MPO and FABP biomarker analysis. Information on the synthesis, purification, and expression analysis of anti-MPO and anti-FABP scFv is given in the supporting information SI1-SI4.

In order to ascertain the analyte binding performance of scFv anti-MPO and anti-FABP, a standard half maximal inhibitory concentration analysis (IC50) was carried out using an ELISA protocol. IC50 measurements were carried out by competing immobilised anti-FABP and anti-MPO scFv with solution-phase FABP and MPO are shown in figures 3a and 3b. The binding activity was evaluated by the IC50: the concentration at which half-maximum inhibition of antibody-antigen interactions by the competing antigen is achieved. With the indirect competition ELISA, the obtained values of IC50 for anti-hFABP and anti-MPO scFv were approximately 16 and 500 ng/mL, respectively. The limit of detection (LoD) for anti-hFABP and the anti-MPO scFv were approximately 2 and 31 $ng.ml^{-1}$, respectively. The results suggested that although the ELISA with scFv give better sensitivities than their regular counterparts (80 and 50 $ng.ml^{-1}$ for FABP and MPO, respectively), LoD remain within or just below the healthy ranges of FABP (1-30 $ng.ml^{-1}$) and MPO (40-80 $ng.ml^{-1}$).[38-43] After the ELISA-based analysis of scFv recombinant proteins, electrical bioassays using the graphene-coated nanoIDE-arrays were carried out. Figure 4 shows the sensor platform assembled and measurements carried out for 'label-free' sensing of FABP and MPO in a buffer solution with physiological salt concentrations (phosphate buffer with an ionic strength of 154 mM). Figure 4a and 4b show photographs of the complete sensor system, where the sensor chip is mounted on to a PCB, encapsulated with a fluidic

reservoir, and connected to external electrical contacts. For sensing experiments, an alternating current (AC) bias was applied between the source and drain electrodes against a reference which is provided by an Ag/AgCl reference electrode mounted at a fixed position in the center of the fluidic reservoir. Source and Drain IDEs are connected by the transducer graphene layer causing an electrical resistance ($R_G$). Total impedance (Z) of devices is recorded in order to carry out impedimetric sensing of FABP and MPO. Six different concentrations of FABP (1 pg.ml$^{-1}$, 500 pg.ml$^{-1}$, 1 ng.ml-1, 10 ng.ml-1, 100 ng.ml$^{-1}$ and 1 µg/ml$^{-1}$) and 7 different concentrations of MPO (1 pg.ml$^{-1}$, 1 ng.ml$^{-1}$, 10 ng.ml$^{-1}$, 100 ng.ml$^{-1}$, 500 ng.ml$^{-1}$, 1 µg/ml$^{-1}$ and 3 µg/ml$^{-1}$) were prepared in the high ionic strength (150 mM) phosphate buffer to use as sample solutions. Impedance of the scFv-modified graphene-coated IDE-array chips was measured after pipetting 400 µl sample solution for each concentrations and after incubation for 10 minutes. Figure 4c and 4d show the impedance behavior of anti-FABP scFv-modified graphene-coated nanoIDEs-based and microIDEs-based senor chips, respectively. Measurements were performed by applying a sinusoidal perturbation potential of 100 mV rms vs. the open circuit potential in a frequency range from 1 Hz-10 kHz between the source and drain IDE-array contacts lines. The impedance behavior of the sensor chips clearly shows a consistent increase of impedance with increasing concentration of MPO. It is interesting to note that the impedance behavior of the graphene-nanoIDE-arrays was significantly different towards the higher frequencies (> 3 kHz) as compared to graphene-microIDE-arrays, which may be due to higher capacitive load in the nanoscale sensors. Differential transfer function measurements of graphene-coated nanoIDE-arrays and microIDE-arrays against a frequency modulated electrochemical bias carried out in different ionic strengths also showed higher frequency cut-offs for graphene-coated nanoIDE-arrays (supporting information SI9). The impedance behavior of the anti-MPO-modified graphene- coated nanoIDE-arrays and microIDE-arrays upon introducing different concentrations of MPO is shown in figures 4e and 4f. The impedance behavior was recorded for frequencies ranging from 1Hz to 10kHz, showing consistent increase in the impedance with increase of MPO concentrations. It is to be noticed that although the device-to-device variation in impedance values on a sensor chip were very low (figure 5), the graphs in the figure 4 show measurements of devices from different chips resulting in

variations in impedance values coming from slight differences in the graphene transfer and cleaning processes during the assembly of sensor platform.

Figure 5 summarizes the biosensor response of graphene-coated nanoIDE-arrays and microIDE-arrays and compares the performance of our electrical bioassays with the classical ELISA-based approaches. All the graphs from 5a to 5d show average impedance values from 16 individual channels on a sensor chip recorded at 30 Hz (red dots connected with red dashed line). The pink background represents tentative FABP and MPO biomarker concentrations of clinical relevance in humans on the x-axis, while the red and blue dash-dot vertical lines show LoD values for conventional ELISA based protocols reported in literature and ELISA screening with scFV, respectively. The graphene-coated IDE sensors showed a wide dynamic range from $pg.ml^{-1}$ to $\mu g.ml^{-1}$ concentrations, with a sigmoidal dose response curve for both MPO and FABP biomarkers. As it can be seen from the graphs shown in figure 5, the sensors showed promising performance with the FABP assay demonstrating an almost linear response in the clinically-relevant concentration range for the micro-IDE sensors. However, for real clinical applications, a further improvement of our sensor platform is needed. Especially, the relatively small clinically relevant concentration range for MPO requires an optimized resolution in this range, where the nanoIDE sensor might have the best potential to meet this demand (see figure 5c). Graphene-coated nanoIDE-arrays without biofunctionalization were used for negative control of the bioassays developed here for the detection of FABP and MPO in physiological saline which is shown in the supporting information (SI10).

## Conclusion

In this manuscript, we present a new electrical biosensor platform provided by fabrication of nanoscale and microscale IDE-arrays using top-down nanoimprint lithography and photolithography methods and, subsequently, transferring graphene as a 2D transducer material. The graphene-coated nanoIDE and microIDE-array-based devices were surface factionalized with scFv recombinant antibody fragments for efficient binding of FABP and MPO, important cardiovascular disease biomarkers. The assembled sensor platform showed high-performance sensor characteristics with very low device-to-device variations. Most importantly, sensors were deployable in physiological buffers

for ‘label-free’ screening of large protein molecules such as FABP and MPO. Limitations of optical and other sensing approaches in detection of very low concertation of such biomarkers in complex media is a significant challenge to overcome in order to realize ‘point-of-care’ platforms for clinical diagnostics. Wide sensor dynamic ranges beyond clinically relevant concentration ranges demonstrated by our sensor platform together with very low LoD at $pg.ml^{-1}$ concentrations of FABP and MPO in physiological buffers are expected to provide a significant thrust in the development of electrical assays for clinical applications. Our sensor approach is expected to aid in the development of further healthcare diagnostic solutions in high-risk patients suffering from cardiovascular patients as well as enable the realization of personalized diagnostics platforms for regular health monitoring.

## Materials and Methods

***Electrical Assays:*** Sensor chips with NanoIDE and microIDE-arrays were fabricated in a top-down lithography approach with a combination of nanoimprint and lithography process on $Si/SiO_2$ wafers. The process flow of the nanofabrication process and further details are given in the supporting information. The graphene layers were grown in a chemical vapor deposition (CVD) process over 2" x 2" copper substrates. The graphene transfer onto the sensor chips was carried out using a solution-based process with polystyrene as a polymer support.[44] In brief, graphene covered copper foils were coated with polystyrene film and cut into small sizes (approx. 3 x 3 mm) which was sufficient to cover all the 16 nanoIDE or microIDE-array channels on the sensor chips. To prepare the polymer film, typically a polystyrene bead weighing around 0.07 grams was dissolved in 3 ml toluene procured from Sigma Aldrich, Germany and drop casted on top of the graphene-coated copper foil. The polymer-coated graphene foils were baked for 5 minutes in a convection oven at 95 °C. Polystyrene-coated foils were carefully transferred to a copper etching bath made up of 2.5 ml $H_2O_2$, 7.5 ml HCl (both Sigma Aldrich, Germany) and 42 ml deionized water. Foils are left floating on the solution surface for copper etching resulting in polystyrene films with graphene layer sticking underneath. The graphene layer with the polystyrene film on top was transferred to a water bath for cleaning and then fished out by placing sensor chips under the floating graphene layer in appropriate orientation so as to cover the nanoIDE or microIDE-arrays. After immobilizing the polystyrene-coated graphene onto the sensor areas, the sensor chips were placed in toluene solution for 2 hours on a shaker to wash off the polystyrene layer from the graphene. Before graphene transfer, sensor chips were cleaned using ultrasonication in acetone, isopropanol and distilled water (5 min each) and subsequently by plasma cleaning in an oxygen plasma chamber (Diener Electronic, Germany) at 0.6 mbar, 140 Watts for 5 min. After graphene transfer, the sensor chips were annealed at 350 °C for 2 h in an argon atmosphere.

Topographical characterization of the sensor chips was carried out using scanning electron microscopy (Zeiss Supra 40 SEM, Carl Zeiss AG), atomic force microscopy (Nanoscope Dimension 3100 AFM, Veeco probes, USA) and Raman microscopy (Horiba LabRam spectrometer). Field-effect

characterization of sensor chips was carried out on a semiconductor parameter analyzer (Keithley 4200-SCS, Tektronix, USA), while impedimetric measurements for transconductance measurements and determination of cut-off frequency were carried out using a home built, 16 channel portable amplifier for dc and ac measurements. The sensor measurements for the detection of h-type FABP and MPO using impedance spectroscopy were carried out on an electrochemical workstation (Zahner Zennium, Zahner Elektrik, Germany).

For biosensor measurements, sensor chips were wire-bonded onto PCBs and encapsulated using a borosilicate glass ring (borosilicate glass 3.3, $d_o$: 9 mm, $d_i$: 7 mm, wall thickness: 1 mm, h: 2 mm, from Becker Glas, Germany) and using a PDMS (Sylgard 184, Dow Corning USA) layer. This glass ring is glued onto the sensor chip surrounding the sensor arrays while a larger glass ring (borosilicate glass 3.3, $d_o$: 20 mm, wall thickness: 1.2 mm, $d_i$: 17.6 mm, h: 3 mm, Becker Glass, Germany) was placed concentrically and covered the wire-bonds connecting the sensor chip with the electrical contact pads of the PCB. The space between the glass rings, which also protected the wire-bonds was filled with PDMS and cured in an oven at 120 °C. With this encapsulation procedure, the gold bonds were completely passivated by PDMS and a small reservoir on top of the sensor area was assembled for easy placement of analyte solutions during analytical measurements. Encapsulated sensor chips were placed onto a plastic-lead chip carrier (PLCC 68 1.27 mm pitch T+B IC51, Yamaichi electronics, Japan) equipped with wire connections addressing channels on the sensor chip, individually.

For bioimmobilization of anti-FABP and anti-MPO scFv recombinant antibody fragments on graphene-coated nanoIDE and microIDE-arrays, sensor chips were treated with 95% 3-mercaptopropyltrimethoxysilane (MPTMS) from Sigma Aldrich, Germany in propanol (1:100 ratio). 40 µl MPTMS solution was placed on the sensor chip for 2 hours, cleaned with propanol-2, and blow-dried with $N_2$ gas. Forty µl solutions of anti-FABP scFv and anti-MPO scFv at 1µg/ml concentrations were placed on the sensor surface and incubated for ~12 hours. After incubation, the immobilization solution was discarded and the sensor surface was rinsed twice with PBS, pH 7.4. FABP and MPO

were detected with a range of concentrations (1 $pg.ml^{-1}$ – 2 $\mu g.ml^{-1}$ MPO and 1 $pg.ml^{-1}$ – 1 $\mu g.ml^{-1}$ FABP) with an incubation of 10 min for each concentration using a volume of 400 µl.

***Competitive ELISA:*** Half-area 96-well plates (Fisher, Ireland) were coated with 30 µL of 2.5 µg/mL hFABP and 2 µg/mL MPO (AMS Biotechnologies, UK) separately and left overnight at 4°C. The plates were then blocked by using 60 µL/well of 5% (w/v) PBSTM at 37°C for one hour, followed with a wash using PBS (60 µL/well). To carry out the competitive ELISA, different concentrations of hFABP (0-500 $ng.ml^{-1}$) or MPO (0-2,000 ng/mL) were prepared and mixed with a fixed concentration of anti-hFABP (0.26 µg/mL) and anti-MPO (0.03 µg/mL) scFv. This mixture (30µL/well) was incubated at room temperature for 10 min and served for the competitive ELISA measurements. For performance of negative control experiments, 30 µL/well of hFABP-free and MPO-free human serum were applied instead of the scFv and antigen mixture. The plates were washed using PBS (60 µL/well) followed with addition of HRP-labelled HA antibody (1:1,000 dilution; 30 µL/well) and incubation at room temperature for 10 min. The plates were washed once again using PBS (60µL/well). TMB in what (0.4 g/L, 30µL/well) was added to the plates and incubated at room temperature for 2 min. The reaction was stopped by addition of 30 µL of 1 M HCl per well. The absorbance of the wells was read at 450 nm using a Safire 2 plate reader.

## Acknowledgements

We thank Prof. K. Balasubramanian for the help with the solution mediated graphene transfer process. This research work was supported by the Stiftung Rheinland-Pfalz für Innovation Nr. 1082.Vivek Pachauri acknowledges the support from Euroimmun AG for funding of his position. We also acknowledge support from European Commission FP7 Programme through the Marie Curie Initial Training Network PROSENSE (grant no. 317420, 2012-2016) and from DCU INVENT and Imperial sources). All the authors thank Detlev Cassel, Andreas Pastille and Walid Munief for their help in the clean-room processes and with the surface characterizations.

**Figures:**

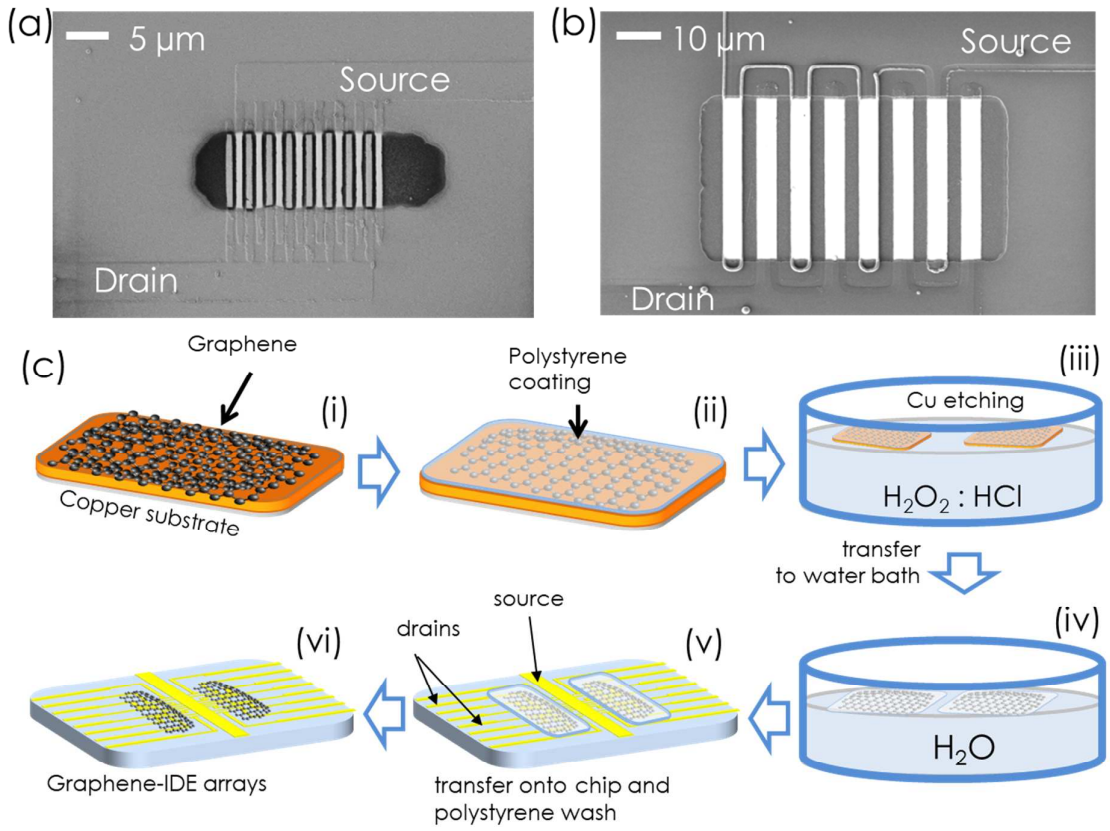


Figure 1: Preparation of graphene-coated nanoIDE and microIDE-array sensor chips. (a) SEM image of a nanoIDE-array chip showing 16 nanoelectrodes with a passivation layer protecting the electrode contacts. (b) SEM scan image of the microIDE-arrays chip showing 8 microelectrodes with a passivation layer. (c) Schematic illustration of the solution-based graphene transfer process from the copper substrate onto the sensor chips using polystyrene support.

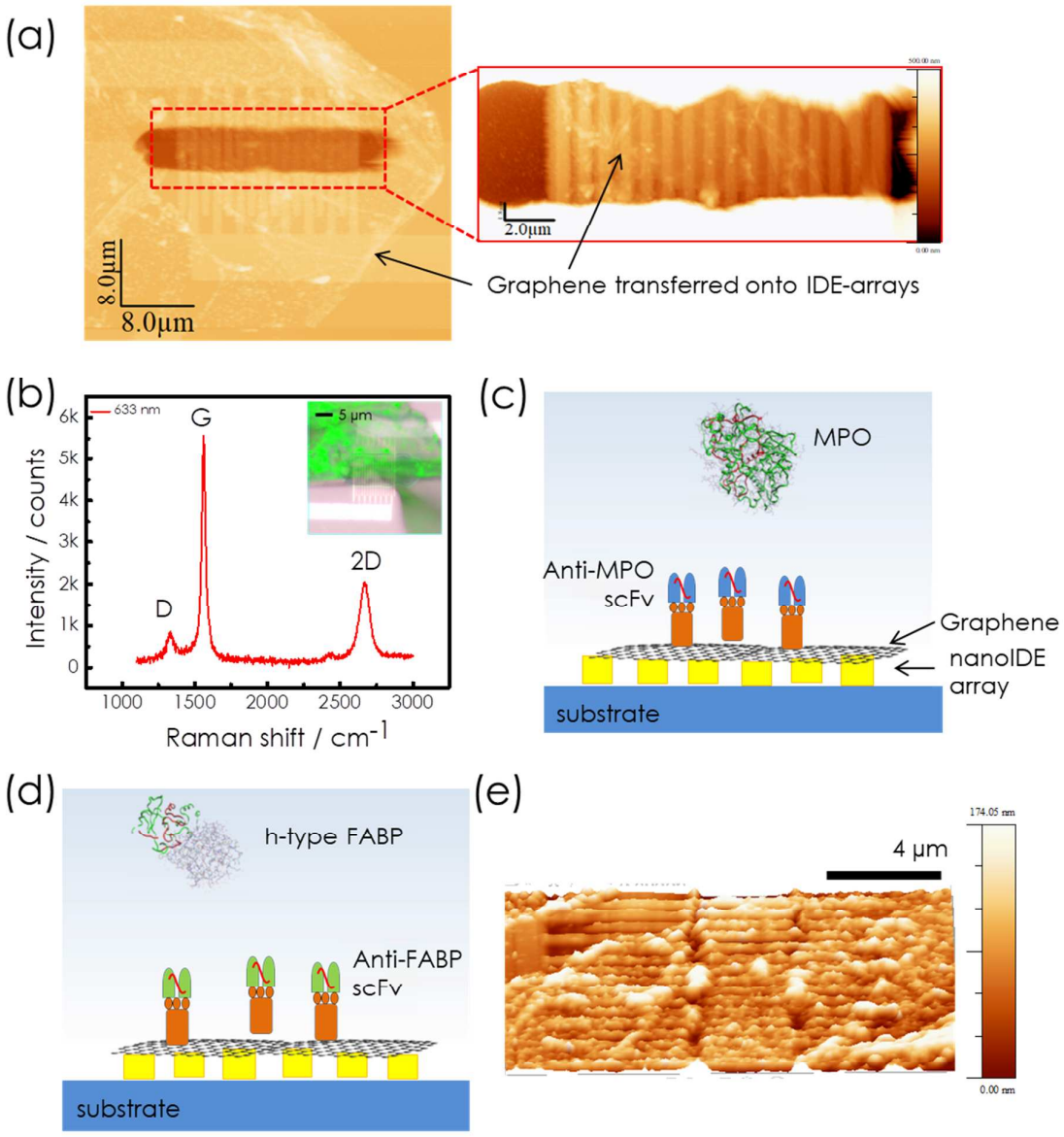


Figure 2: Characterization of the graphene-coated IDE-arrays and assembly of the sensor platform. (a) Atomic force microscopy image of a nanoIDE-array after positioning graphene on top showing a complete coverage of the nanoelectrodes with the graphene layer. (b) The graph shows a typical Raman spectrum of the graphene layer positions on top of nanoIDE-array. The image in the inset represents a characteristic Raman map taken over the sensor-area, whereas the green overlay - represents the G-peak intensities of the graphene layer. (c, d) Schematic illustration of the bioimmobilization of multilayer graphene-coated IDE-arrays chips with anti-MPO and anti-FABP scFv recombinant antibodies, respectively. (e) AFM image of a typical sensor surface after the bioimmobilization process.

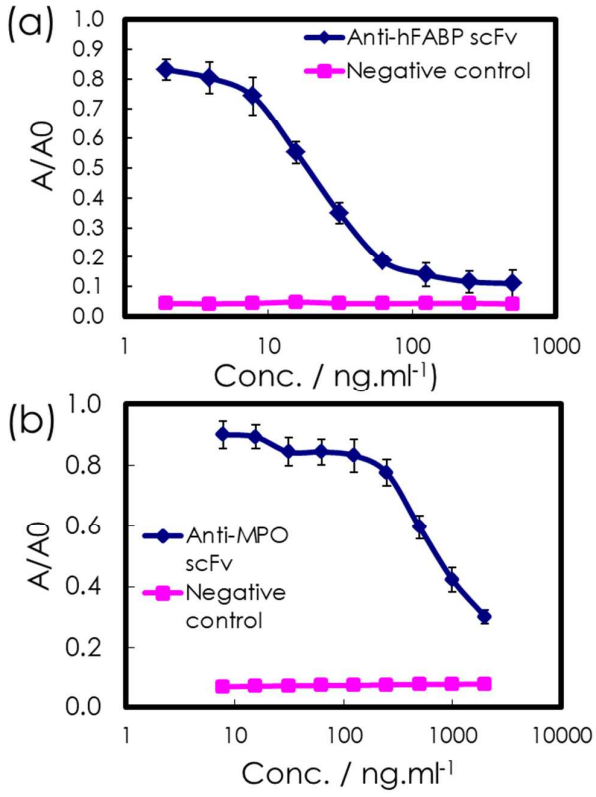


Figure 3: Competitive ELISA showing the limit of detection using (a) anti h-FABP and (b) anti-MPO scFv antibody fragments proteins. Absorbance with no h-FABP or MPO competition is referred to as A0. The absorbance with h-FABP and MPO competition are referred to as A. For the negative control, the absorbance with h-FABP-free and MPO-free sera was used instead of A/A0. The results are shown as the mean ± S.D. (n=3).

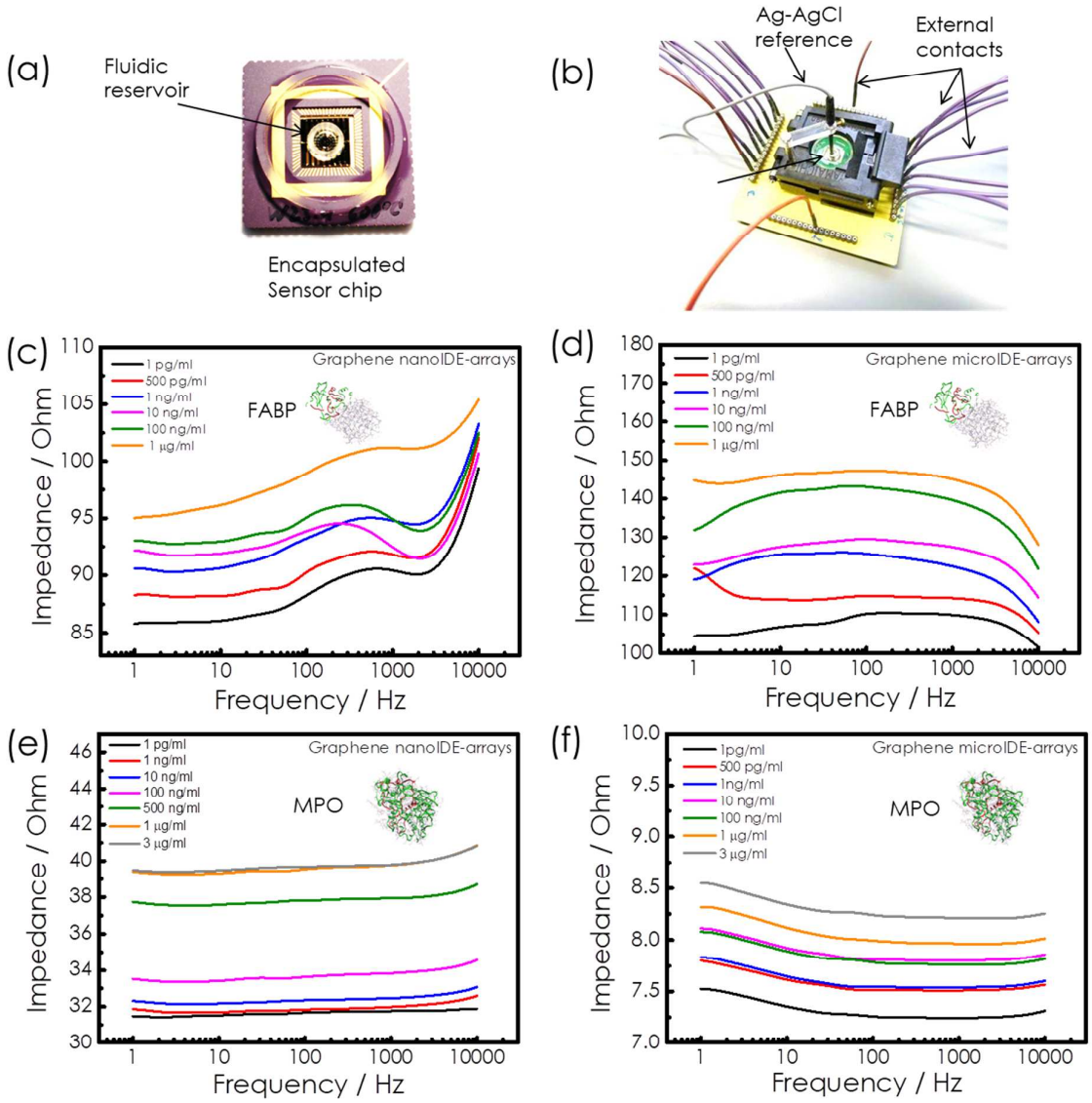


Figure 4: Label-free screening of cardiac disease biomarkers on graphene-coated IDE-arrays. (a, b) The encapsulated sensor chip and the measurement set-up is shown in the photograph, where a sensor-chip is assembled on top of a chip-carrier, encapsulated with a fluidic chamber and connected to external electrical contacts for measurements. An individual sensor chip is shown in the inset. (c, d) In-line impedance spectra of the sensor chips (graphene-coated nanoIDE and microIDE-arrays, respectively) biofunctionalized with anti h-FABP scFv when subjected to different concentrations of h-type FABP in physiological buffer. (e, f) In-line impedance spectra measured for different concentrations of MPO in physiological buffer on the anti-MPO scFv-modified sensor chips.

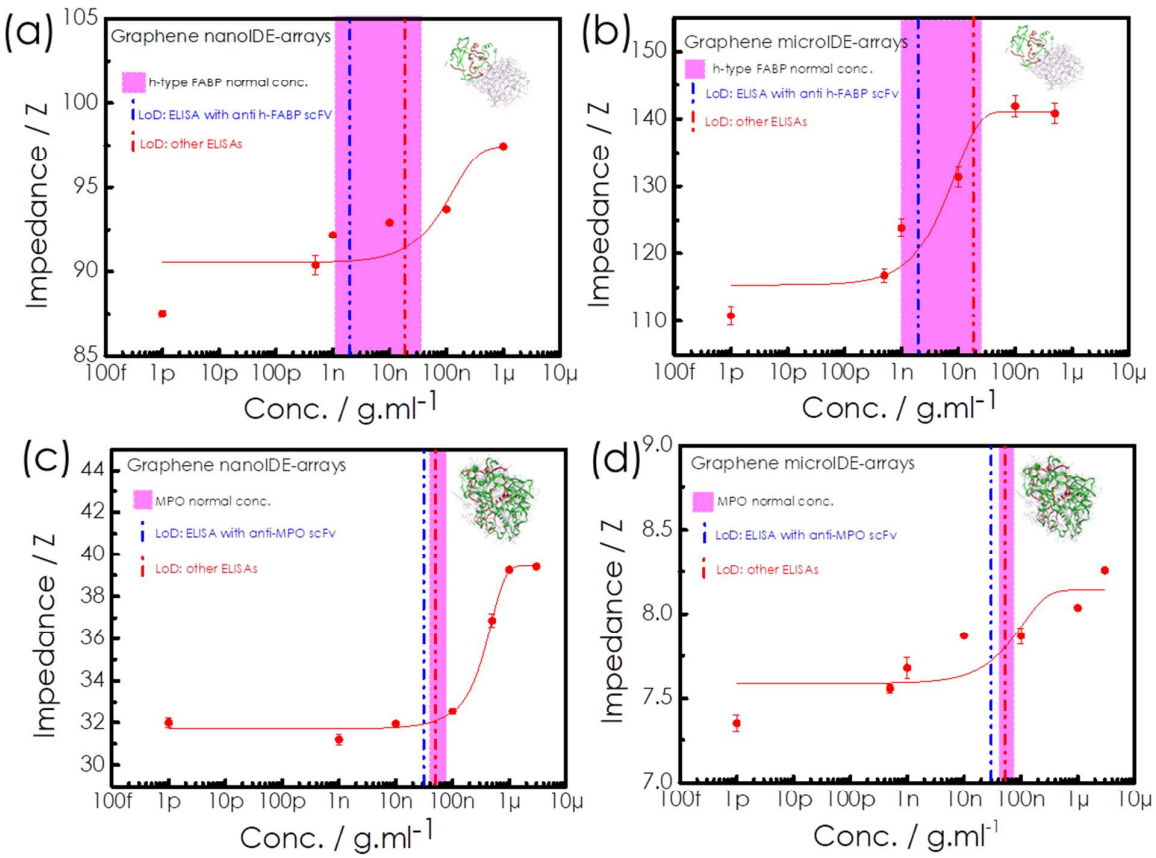


Figure 5: Performances of graphene-coated IDE-arrays sensor platform vis-à-vis ELISA methods for the detection of h-type FABP and MPO. (a) The graph showing a nearly sigmoidal increase in the impedance values (extracted at 30 Hz) of the graphene-coated nanoIDE-array sensors as a function of h-type FABP concentration in the buffer shown as red dots and a dashed line extrapolated in red color. The purple box shows the normal concentration of h-type FABP in humans while the red and blue vertical dash-dot lines show the LoD using state-of-the-art ELISA methods and ELISA procedure using scFv recombinant antibody fragments as used in this study, respectively. (b) Dose-response curve obtained for different h-type FABP concentrations in buffer using graphene-coated microIDE-array sensors and comparison to LoD values from ELISA methods. (c, d) Dose response obtained for different concentrations of MPO using graphene-coated nanoIDE-arrays and microIDE-arrays, respectively, and comparison of their performance with the ELISA-based approaches. 16 different devices were measured for each graph shown here.

## References


1. Balakumar, P.; Maung, U. K.; Jagadeesh, G., Prevalence and prevention of cardiovascular disease and diabetes mellitus. *Pharmacological research* **2016,** *113* (Pt A), 600-609.
2. Wilkins, E.; Wilson, L.; Wickramasinghe, K.; Bhatnagar, P.; Rayner, M.; Townsend, N.; Leal, J.; Luengo-Fernandez, R.; Burns, R. *European Cardiovascular Disease Statistics 2017 edition*; European Heart Network: 2017.
3. Steg, P. G.; James, S. K.; Atar, D.; Badano, L. P.; Blomstrom-Lundqvist, C.; Borger, M. A.; Di Mario, C.; Dickstein, K.; Ducrocq, G.; Fernandez-Aviles, F.; Gershlick, A. H.; Giannuzzi, P.; Halvorsen, S.; Huber, K.; Juni, P.; Kastrati, A.; Knuuti, J.; Lenzen, M. J.; Mahaffey, K. W.; Valgimigli, M.; van 't Hof, A.; Widimsky, P.; Zahger, D., ESC Guidelines for the management of acute myocardial infarction in patients presenting with ST-segment elevation. *Eur Heart J* **2012,** *33* (20), 2569-619.
4. Hozawa, A.; Folsom, A. R.; Sharrett, A.; Chambless, L. E., Absolute and attributable risks of cardiovascular disease incidence in relation to optimal and borderline risk factors: Comparison of african american with white subjects—atherosclerosis risk in communities study. *Archives of Internal Medicine* **2007,** *167* (6), 573-579.
5. Wang, J.; Tan, G. J.; Han, L. N.; Bai, Y. Y.; He, M.; Liu, H. B., Novel biomarkers for cardiovascular risk prediction. *Journal of geriatric cardiology : JGC* **2017,** *14* (2), 135-150.
6. Savic-Radojevic, A.; Pljesa-Ercegovac, M.; Matic, M.; Simic, D.; Radovanovic, S.; Simic, T., Chapter Four - Novel Biomarkers of Heart Failure. In *Advances in Clinical Chemistry*, Gregory, S. M., Ed. Elsevier: 2017; Vol. Volume 79, pp 93-152.
7. Chatterjee, N. A.; Singh, J. P., Novel Interventional Therapies to Modulate the Autonomic Tone in Heart Failure. *JACC. Heart failure* **2015,** *3* (10), 786-802.
8. Fang, Y., Are label-free investigations the best approach to drug discovery? *Future Medicinal Chemistry* **2015,** *7* (12), 1561-1564.
9. Lippi, G.; Mattiuzzi, C.; Cervellin, G., Critical review and meta-analysis on the combination of heart-type fatty acid binding protein (H-FABP) and troponin for early diagnosis of acute myocardial infarction. *Clinical biochemistry* **2013,** *46* (1-2), 26-30.
10. Otaki, Y.; Takahashi, H.; Watanabe, T.; Yamaura, G.; Funayama, A.; Arimoto, T.; Shishido, T.; Miyamoto, T.; Kubota, I., Heart-type fatty acid binding protein and high-sensitivity troponin T are myocardial damage markers that could predict adverse clinical outcomes in patients with peripheral artery disease. *BBA clinical* **2015,** *4*, 35-41.
11. Azzazy, H. M.; Pelsers, M. M.; Christenson, R. H., Unbound free fatty acids and heart-type fatty acid-binding protein: diagnostic assays and clinical applications. *Clinical chemistry* **2006,** *52* (1), 19-29.
12. Kaczynska, A.; Pelsers, M. M.; Bochowicz, A.; Kostrubiec, M.; Glatz, J. F.; Pruszczyk, P., Plasma heart-type fatty acid binding protein is superior to troponin and myoglobin for rapid risk stratification in acute pulmonary embolism. *Clinica chimica acta; international journal of clinical chemistry* **2006,** *371* (1-2), 117-123.
13. Huston, J. S.; Levinson, D.; Mudgett-Hunter, M.; Tai, M.-S.; Novotny, J.; Margolies, M. N.; Ridge, R. J.; Bruccoleri, R. E.; Haber, E.; Crea, R.; Oppermann, H., Protein engineering of antibody binding sites: Recovery of specific activity in an anti-digoxin single-chain Fv analogue produced in Escherichia coli. *Proc. Natl. Acad. Sci. USA* **1988,** *85*, 5879-5883.
14. Holliger, P.; Hudson, P. J., Engineered antibody fragments and the rise of single domains. *Nature biotechnology* **2005,** *23* (9), 1126-36.
15. Ayyar, B. V.; Hearty, S.; O'Kennedy, R., Highly sensitive recombinant antibodies capable of reliably differentiating heart-type fatty acid binding protein from noncardiac isoforms. *Analytical biochemistry* **2010,** *407* (2), 165-71.
16. Ma, H.; O'Kennedy, R., *Recombinant Antibody Fragment Production*. 2016.
17. Bellan, L. M.; Wu, D.; Langer, R. S., Current trends in nanobiosensor technology. *Wiley interdisciplinary reviews. Nanomedicine and nanobiotechnology* **2011,** *3* (3), 229-46.

18. Connolly, P., Clinical diagnostics opportunities for biosensors and bioelectronics. *Biosensors & bioelectronics* **1995,** *10*, 1-6.
19. Pickup, J. C., Biosensors: A clinical Perspective. *The Lancet* **1985**, 817-820.
20. Damen, J. A.; Hooft, L.; Schuit, E.; Debray, T. P.; Collins, G. S.; Tzoulaki, I.; Lassale, C. M.; Siontis, G. C.; Chiocchia, V.; Roberts, C.; Schlussel, M. M.; Gerry, S.; Black, J. A.; Heus, P.; van der Schouw, Y. T.; Peelen, L. M.; Moons, K. G., Prediction models for cardiovascular disease risk in the general population: systematic review. *Bmj* **2016,** *353*, i2416.
21. Schroeder, F.; Jolly, C. A.; Cho, T.-H.; Frolov, A., Fatty acid binding protein isoforms: structure and function. *Chemistry and Physics of Lipids* **1998,** *92*, 1-25.
22. Ahmad, Z. A.; Yeap, S. K.; Ali, A. M.; Ho, W. Y.; Alitheen, N. B.; Hamid, M., scFv antibody: principles and clinical application. *Clinical and Developmental Immunology* **2012,** *2012*, 980250.
23. Shearer, C. J.; Slattery, A. D.; Stapleton, A. J.; Shapter, J. G.; Gibson, C. T., Accurate thickness measurement of graphene. *Nanotechnology* **2016,** *27* (12), 125704.
24. Ferrari, A. C.; Basko, D. M., Raman spectroscopy as a versatile tool for studying the properties of graphene. *Nature nanotechnology* **2013,** *8*, 235-246.
25. Cong, C.; Yu, T., Evolution of Raman G and G′(2D) modes in folded graphene layers. *Physical Review B* **2014,** *89* (23).
26. Das, A.; Chakraborty, B.; Sood, A. K., Raman spectroscopy of graphene on different substrates and influence of defects. *Bull. Mater. Sci.* **2008,** *31* (3), 579–584.
27. Park, K.; Ryu, S., Direction-controlled chemical doping for reversible G-phonon mixing in ABC trilayer graphene. *Scientific reports* **2015,** *5*, 8707.
28. Pachauri, V.; Ingebrandt, S., Biologically sensitive field-effect transistors: from ISFETs to NanoFETs. *Essays in biochemistry* **2016,** *60* (1), 81-90.
29. Balasubramanian, K.; Kern, K., 25th anniversary article: label-free electrical biodetection using carbon nanostructures. *Advanced materials* **2014,** *26* (8), 1154-75.
30. Hinchet, R.; Kim, S. W., Patient-Inspired Engineering and Nanotechnology. *ACS Nano* **2015,** *9* (8), 7742-5.
31. Biju, V., Chemical modifications and bioconjugate reactions of nanomaterials for sensing, imaging, drug delivery and therapy. *Chemical Society reviews* **2014,** *43* (3), 744-64.
32. Oliveira Jr., O. N.; Iost, R. M.; Siqueira Jr., J. R.; Crespilho, F. N.; Caseli, L., Nanomaterials for diagnosis: challenges and applications in smart devices based on molecular recognition. *ACS applied materials & interfaces* **2014,** *6* (17), 14745-66.
33. Baker, M., Blame it on the Antibodies. *Nature* **2015,** *521*, 274-276.
34. O'Sullivan, C. K., Aptasensors--the future of biosensing? *Analytical and bioanalytical chemistry* **2002,** *372* (1), 44-8.
35. Lee, J. O.; So, H. M.; Jeon, E. K.; Chang, H.; Won, K.; Kim, Y. H., Aptamers as molecular recognition elements for electrical nanobiosensors. *Analytical and bioanalytical chemistry* **2008,** *390* (4), 1023-32.
36. Luo, X.; Davis, J. J., Electrical biosensors and the label free detection of protein disease biomarkers. *Chemical Society reviews* **2013,** *42* (13), 5944-62.
37. Spain, E.; Gilgunn, S.; Sharma, S.; Adamson, K.; Carthy, E.; O'Kennedy, R.; Forster, R. J., Detection of prostate specific antigen based on electrocatalytic platinum nanoparticles conjugated to a recombinant scFv antibody. *Biosensors & bioelectronics* **2016,** *77*, 759-766.
38. Ishimura, S.; Furuhashi, M.; Watanabe, Y.; Hoshina, K.; Fuseya, T.; Mita, T.; Okazaki, Y.; Koyama, M.; Tanaka, M.; Akasaka, H.; Ohnishi, H.; Yoshida, H.; Saitoh, S.; Miura, T., Circulating levels of fatty acid-binding protein family and metabolic phenotype in the general population. *PloS one* **2013,** *8* (11), e81318.
39. Otaki, Y.; Watanabe, T.; Takahashi, H.; Hirayama, A.; Narumi, T.; Kadowaki, S.; Honda, Y.; Arimoto, T.; Shishido, T.; Miyamoto, T.; Konta, T.; Shibata, Y.; Fukao, A.; Daimon, M.; Ueno, Y.; Kato, T.; Kayama, T.; Kubota, I., Association of Heart-Type Fatty Acid-Binding Protein with Cardiovascular

Risk Factors and All-Cause Mortality in the General Population: The Takahata Study. *PloS one* **2014,** *9* (5), 10.

40. Esporcatte, R.; Rey, H. C. V.; Rangel, F. O. D.; Rocha, R. M.; de Mendonça Filho, H. T. F.; Dohmann, H. F. R.; Filho, F. M. A., Predictive value of myeloperoxidase to identify high risk patients admitted to the hospital with acute chest pain. *Arq Bras Cardiol.* **2007,** *89* (6), 377-84.

41. Mocatta, T. J.; Pilbrow, A. P.; Cameron, V. A.; Senthilmohan, R.; Frampton, C. M.; Richards, A. M.; Winterbourn, C. C., Plasma concentrations of myeloperoxidase predict mortality after myocardial infarction. *Journal of the American College of Cardiology* **2007,** *49* (20), 1993-2000.

42. Goiffon, R. J.; Martinez, S. C.; Piwnica-Worms, D., A rapid bioluminescence assay for measuring myeloperoxidase activity in human plasma. *Nature communications* **2015,** *6*, 6271.

43. Wodzigl, K. W. H.; Pelsersl, M. M. A. L.; van der Vussel, G. J.; Roos, W.; Glatz, J. F. C., One-step enzyme-linked immunosorbent assay (ELISA) for plasma fatty acid-binding protein. *Ann Clin Biochem* **1997,** *34*, 263-268.

44. Yu, H. K.; Balasubramanian, K.; Kim, K.; Lee, J.-L.; Maiti, M.; Ropers, C.; Krieg, J.; Kern, K.; Wodtke, A. M., Chemical Vapor Deposition of Graphene on a “Peeled-Off” Epitaxial Cu(111) Foil: A Simple Approach to Improved Properties. *ACS Nano* **2014,** *8* (8), 8636–8643.